

# Robust Vibration Suppression Control Profile Generation Based on Time-Frequency Uncertainty

Li Zhou  
 School of Mechanical and Aerospace  
 Engineering  
 Oklahoma State University  
 Stillwater, OK 74078-5016, USA  
 zhoul@acl.okstate.edu

Eduardo A. Misawa  
 School of Mechanical and Aerospace  
 Engineering  
 Oklahoma State University  
 Stillwater, OK 74078-5016, USA  
 misawa@okstate.edu

**Abstract**— In this paper, a robust control profile is generated which suppresses all the high frequency resonant dynamics in a flexible dynamic system. This robust control profile is the shifted time-limited version of the functions that optimally achieve the time-frequency localization. The robust control profile is optimized by considering the first resonance mode through the filter theory. The simulation results for hard disk drive seek control show the effectiveness of the proposed method.

## I. INTRODUCTION

Control of flexible structures has been studied extensively in recent years. Flexible structures such as high-speed disk drive actuators require high precision positioning under tight time constraints. Whenever a fast motion is commanded, residual vibration in the flexible structure is induced, which increases the settling time. One solution is to design a closed-loop control to damp out vibrations caused by the command inputs and disturbances to the plant. However, the resulting closed-loop damping ratio may still be too slow to provide acceptable settling time. Also, the closed-loop control is not able to compensate for high frequency residual vibration which occurs beyond the closed-loop bandwidth. An alternative approach is to develop an appropriate reference trajectory that can minimize the excitation energy imparted to the system at its natural frequencies.

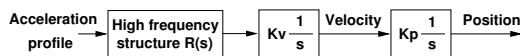


Fig. 1. Typical mechanical flexible system scheme.

Fig. 1 shows a typical mechanical flexible system, where  $\frac{1}{s}$  is an integrator,  $Kv$  is a velocity constant gain, and  $Kp$  is a position constant gain. The high frequency modes can be described as a transfer function  $R(s)$  which has possibly infinite number of lightly damped resonant structures,

$$R(s) = \lim_{n \rightarrow \infty} \frac{b_n s^n + b_{n-1} s^{n-1} + \dots + b_1 s + 1}{a_n s^n + a_{n-1} s^{n-1} + \dots + a_1 s + 1}. \quad (1)$$

Robust vibration suppression trajectory generation is to find a fast input trajectory, under some physical constraint, with minimum possible residual vibration.

One of the pioneering works of the shaped function synthesis was introduced by Aspinwall [1], who used a finite Fourier series expansion to construct forcing functions to attenuate the residual dynamic response for slewing a flexible

beam. The response spectrum envelope is made small only in a limited region. Also the forcing functions are sensitive to the control system. Another pioneering work was introduced by Swigert [2], who used a performance index which reflects the concern for the accuracy of the terminal boundary conditions to the changes in mode eigen-frequencies. However, the control inputs are difficult to calculate, and only a few modes are considered. Recently, Junkins et al. [3] developed a near minimum-time input with shape control weighting functions. Bhat [4] have shown that control waveforms can be optimized using the Laplace domain synthesis technique. But the control inputs need to be assumed through a judicious choice.

None of the previous methods consider all the resonance modes, which in reality may be infinite in number. Also, the modes' responses change drastically due to resonance modeling uncertainty. To overcome the resonance frequency variation, Yamamura and Ono [5] have developed a robust vibrationless control solution derived for an enlarged multi-degree-of-freedom system that has some virtual frequencies within the range of the varying natural frequencies. Meckl and Roberto [6] followed the same approach and developed a forcing function using a series of ramped sinusoids for one nominal resonance model. The spectrum magnitude of the forcing function becomes small at the nominal resonance frequency and the four additional frequencies surrounding the nominal frequency. But the spectrum magnitude of the forcing function increases significantly at frequencies beyond these.

In the more recent work of Yamamura and Ono [7], [8], [9], the authors described a frequency-shaped cost functional whose weighting function was represented by a first-order and second-order high-pass filter in the design of vibrationless access control forces. The control forces have small frequency components in the high frequency region. But the decay rate in the frequency domain depends on the shape of the weighting function. Mizoshita et al. [10] developed an access control called SMART (Structural Vibration Minimized Acceleration Trajectory) for hard disk drives. The access formula is derived from the minimum-jerk cost function where the SMART state values (position, velocity, and acceleration) are expressed using time polynomials. But the jerk cost function has no direct relationship to the residual vibration.

The paper is organized as follows. The next section describes the time-frequency localization problem. The section that follows then develops the new design approach based on the functions which optimally achieve the time-frequency localization. The control profile based on the optimal functions is optimized with a scale parameter to guarantee the energy of the control profile is concentrated in a specified low frequency interval. Next, simulation results for a hard disk drive open-loop seek control are presented. The paper closes with conclusions.

## II. TIME-FREQUENCY LOCALIZATION

In theory, the most efficient way to reduce the move time is to use the time-optimal control input which has the bang-bang form. In practice, to suppress the high frequency residual vibration, the control input must have a small energy distribution at high frequencies (i.e. the control input should behave like an ideal low-pass filter.) However a signal cannot be found using existing techniques which achieves the two properties simultaneously. The following analysis clearly shows this phenomenon. Fig. 2 shows the typical time-optimal command and its spectrum magnitude. The time-optimal command has a sharp decay in the time domain but a very slow decay in the frequency domain. From the top plot in Fig. 2, the time-optimal command suddenly changes from zero to maximum at time zero and suddenly changes from minimum to zero at the end of the command. From the bottom plot in Fig. 2, the magnitude spectrum of the time-optimal command slowly changes its amplitudes from 0 rad/sec to the extremely high frequency. So the total energy of the time-optimal command concentrates in the time domain but spreads over all in the frequency domain. Fig. 3 shows the typical ideal low-pass filter function and its spectrum. Similarly, the ideal low-pass filter function has a sharp decay in the frequency domain but a very slow decay in the time domain. So both bang-bang form forcing function and low-pass filter function are not suitable for robust vibration suppression profile generation.

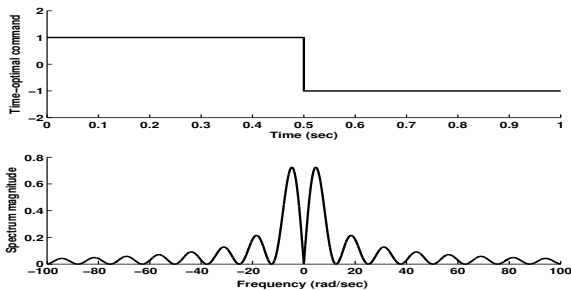


Fig. 2. Time-optimal command input and its spectrum magnitude.

In the communication field, it is known that one cannot simultaneously confine a function  $h(t)$  and its Fourier transform  $H(\omega)$  too strictly. This phenomenon is clearly stated

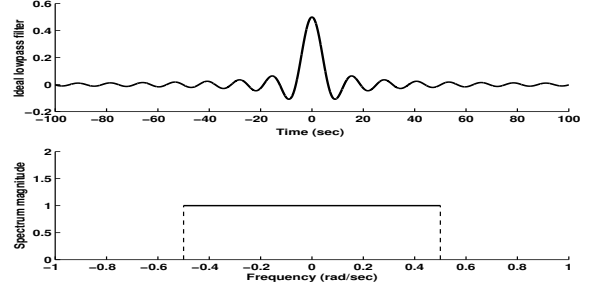


Fig. 3. Ideal low-pass filter function and its Fourier transform.

by the Heisenberg Uncertainty Principle: if the time-spread  $\Delta_{h(t)}$  of  $h(t)$  is measured by

$$\Delta_{h(t)}^2 = \frac{\int_{-\infty}^{\infty} (t - t^*)^2 |h(t)|^2 dt}{\int_{-\infty}^{\infty} |h(t)|^2 dt}, \quad (2)$$

and the frequency-spread  $\Delta_{H(\omega)}$  of  $H(\omega)$  is measured by

$$\Delta_{H(\omega)}^2 = \frac{\int_{-\infty}^{\infty} (\omega - \omega^*)^2 |H(\omega)|^2 d\omega}{\int_{-\infty}^{\infty} |H(\omega)|^2 d\omega}, \quad (3)$$

where  $t^*$  is defined as center of  $h(t)$  and  $\omega^*$  is defined as center of  $H(\omega)$  by

$$t^* = \frac{\int_{-\infty}^{\infty} t |h(t)|^2 dt}{\int_{-\infty}^{\infty} |h(t)|^2 dt} \quad (4)$$

and

$$\omega^* = \frac{\int_{-\infty}^{\infty} \omega |H(\omega)|^2 d\omega}{\int_{-\infty}^{\infty} |H(\omega)|^2 d\omega}. \quad (5)$$

Then the function  $h(t)$  must satisfy the inequality

$$\Delta_{h(t)} \Delta_{H(\omega)} \geq \frac{1}{2}. \quad (6)$$

Thus,  $\Delta_{h(t)}$  and  $\Delta_{H(\omega)}$  cannot, for any Fourier transform pair, be both small. Furthermore, the equality in (6) will hold if and only if  $h(t)$  (and hence  $H(\omega)$ ) are Gaussian [11], [12].

$$h(t) = ce^{iat} e^{-\frac{(t-b)^2}{4\alpha}} \quad (7)$$

for some real constants  $a, b, c$ , and  $\alpha$  with  $a > 0$  and  $c \neq 0$ . In the case of  $b = 0$ , both  $t^*$  and  $\omega^*$  are zero.

In the engineering field,  $2\Delta_{h(t)}$  is called the root mean square (RMS) duration of  $h(t)$ , and  $2\Delta_{H(\omega)}$  is called the RMS bandwidth of the function  $h(t)$ .

Let  $a = 0$  make (7) a real function and let  $c = 1, b = 0$  and  $\alpha = \frac{1}{2}$  reduce (7) to a simple form

$$h(t) = e^{-\frac{t^2}{2}}. \quad (8)$$

The derivative of  $h(t)$  in (8) is given by

$$\phi(t) = -te^{-\frac{t^2}{2}}. \quad (9)$$

The derivative of  $\phi(t)$  in (9) is given by

$$\frac{d}{dt}\phi(t) = -(1-t^2)e^{(-\frac{1}{2}t^2)}, \quad (10)$$

which is the equation for the so-called Mexican hat wavelet.

Fig. 4 shows the waveform of (9) and its spectrum magnitude. It is clear that  $\phi(t)$  decays very quickly both in the time domain and the frequency domain. It also demonstrates that the total energy of  $\phi(t)$  concentrates locally near zero.

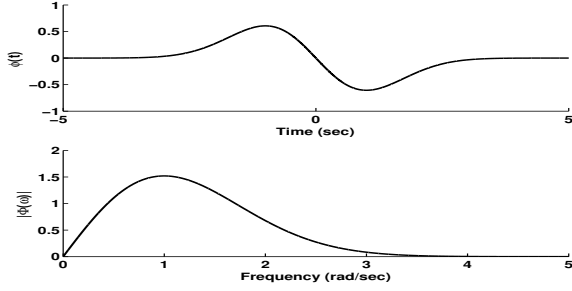


Fig. 4. Function  $-te^{-\frac{t^2}{2}}$  and its spectrum magnitude.

Since the value of  $\phi(t)$  is negligibly small as  $|t|$  becomes bigger,  $\phi(t)$  may be truncated at the range of  $-D \leq t \leq D$  to obtain a time-limited version of  $\phi(t)$ , then shifted forward to make the start time equal to zero and end time equal to  $2D$  as in (11).

$$g_\phi(t) = \begin{cases} \phi(t-D), & \text{if } 0 \leq t \leq 2D; \\ 0, & \text{otherwise.} \end{cases} \quad (11)$$

So  $g_\phi(t)$  can be used as an acceleration candidate for a double integrator system. To guarantee the position constraint, a constant gain  $K$  must be multiplied by the waveform of  $g_\phi(t)$ . Since  $\phi(t)$  decays rapidly as  $t$  increases, the energy distribution of  $g_\phi(t)$ , which is the shifted time-limited version of  $\phi(t)$ , approaches the energy distribution of  $\phi(t)$ . So, if the resonance frequencies of the flexible structure are located at the region where the spectrum of  $g_\phi(t)$  is negligibly small,  $g_\phi(t)$  can suppress residual vibrations of the flexible system. In this case, most of the energy of  $g_\phi(t)$  concentrates before the first resonance frequency, so it can suppress the residual vibration caused by all the resonance modes.

### III. ROBUST VIBRATION SUPPRESSION CONTROL PROFILE DESIGN

Considering the similar waveforms of  $\phi(t)$  but with a different time localization and frequency localization, a scaled version of (9) may be introduced as

$$\phi_n(t) = -te^{(-\frac{1}{2}2^{(2n)}t^2)}, \quad (12)$$

where  $n$  is a real number. When  $n = 0$ , (12) reduces to (9).

Note the following properties of  $\phi_n(t)$ : The maximum of  $\phi_n(t)$  is  $\frac{e^{-1/2}}{2^n}$ , which is achieved at time  $-\frac{1}{2^n}$ . The minimum

of  $\phi_n(t)$  is  $-\frac{e^{-1/2}}{2^n}$ , which is achieved at  $t_m = \frac{1}{2^n}$ . So, as  $n$  increases, the waveform of  $\phi_n(t)$  narrows down to near zero, and the absolute value of  $\phi_n(t)$  decreases. As  $n$  decreases, the waveform of  $\phi_n(t)$  becomes wide and the absolute value of peak of  $\phi_n(t)$  increases.

The continuous-time Fourier transform  $\Phi_n(\omega) = \int_{-\infty}^{\infty} \phi_n(t)e^{-j\omega t} dt$  is given as

$$\Phi_n(\omega) = \frac{j\sqrt{2\pi}\omega e^{(-\frac{1}{2}\frac{\omega^2}{2^{(2n)}})}}{2^{(3n)}}. \quad (13)$$

Note the following properties of  $\Phi_n(\omega)$ : The maximum of  $|\Phi_n(\omega)|$  is  $\frac{\sqrt{2\pi}e^{-1/2}}{2^{(2n)}}$ , which is achieved at  $\omega_m = 2^n$ . As  $n$  increases, the waveform of  $\Phi_n(\omega)$  becomes wide and the maximum of  $|\Phi_n(\omega)|$  decreases. As  $n$  decreases, the waveform of  $\Phi_n(\omega)$  becomes narrow and the maximum of  $|\Phi_n(\omega)|$  increases. Since  $t_m\omega_m = 1$  holds,  $t_m$  and  $\omega_m$  cannot be decreased or increased simultaneously.

Since the value of  $\phi_n(t)$  become negligibly small as  $|t|$  becomes large,  $\phi_n(t)$  may be truncated at the range of  $-D \leq t \leq D$  to obtain a time-limited version of  $\phi_n(t)$ , then shifted forward the waveform to make the start time equal to zero and end time equal to  $2D$  as in (14).

$$g_{\phi,n}(t) = \begin{cases} \phi_n(t-D), & \text{if } 0 \leq t \leq 2D; \\ 0, & \text{otherwise.} \end{cases} \quad (14)$$

So,  $g_{\phi,n}(t)$  can be used as an acceleration profile candidate for a double integrator system. To guarantee the position constraint, a constant gain  $K$  must be multiplied by the waveform  $g_{\phi,n}(t)$ . Since  $\phi_n(t)$  decays rapidly as  $t$  increases, the energy distribution of  $g_{\phi,n}(t)$ , which is the shifted, time-limited version of  $\phi_n(t)$  nears the energy distribution of  $\phi_n(t)$ . So, if the resonance frequencies of the flexible structure are located in the region where the spectrum of  $g_{\phi,n}(t)$  is negligibly small, then  $g_{\phi,n}(t)$  can suppress the residual vibration of the flexible system. In this case, most of the energy of  $g_{\phi,n}(t)$  concentrates before the first resonance frequency, so it can minimize the residual vibration caused by all the resonance modes.

The continuous-time Fourier transform of the truncated version of  $\phi_n(t)$  is very hard to calculate even  $\Phi_n(\omega)$  is very easy to calculate.  $G_{\phi,n}(\omega)$  involves the complex error function, which though is not elaborated on here. In the following analysis, the discrete-time Fourier transform may be used instead of the continuous-time Fourier transform.

Now the discrete-time version of (14) is derived. Assuming the sampling period as  $T_s$  sec and the total discrete-time sequence has  $M+1$  impulses,

$$g_{\phi,n}[k] = \begin{cases} \phi_n((k - \frac{M}{2})T_s), & \text{if } 0 \leq k \leq M; \\ 0, & \text{otherwise.} \end{cases} \quad (15)$$

So the discrete-time sequence  $g_{\phi,n}[k], 0 \leq k \leq M$ , is antisymmetric, and  $\frac{M}{2}$  is the center of symmetry.

When  $M$  is even, the discrete-time Fourier transform  $G_{\phi,n}(\omega) = \sum_{k=-\infty}^{\infty} g_{\phi,n}[k]e^{-j\omega k} = \sum_{k=0}^M g_{\phi,n}[k]e^{-j\omega k}$  can be computed and the magnitude of  $G_{\phi,n}(\omega)$  for even  $M$  is [13]

$$|G_{\phi,n}(\omega)| = \left| 2 \sum_{k=1}^{M/2} \phi_n(-kT_s) \sin(\omega k) \right|. \quad (16)$$

When  $M$  is odd, the discrete-time Fourier transform  $G_{\phi,n}(\omega) = \sum_{k=-\infty}^{\infty} g_{\phi,n}[k]e^{-j\omega k} = \sum_{k=0}^M g_{\phi,n}[k]e^{-j\omega k}$  can be computed and the magnitude value of  $G_{\phi,n}(\omega)$  for odd  $M$  is [13]

$$|G_{\phi,n}(\omega)| = \left| 2 \sum_{k=1}^{(M+1)/2} \phi_n\left(\left(\frac{1}{2} - k\right)T_s\right) \sin(\omega(k - 1/2)) \right|. \quad (17)$$

In contrast to the continuous-time Fourier transform of  $g_{\phi,n}(t)$ , the discrete-time Fourier transform of  $g_{\phi,n}[k]$  can be easily calculated.

Given a fixed move time, the acceleration profile can be determined after choosing the scaling parameter  $n$ . The value of  $n$  can be optimized from the characteristics of the uncertain resonance structure. From the Bode magnitude plot of the resonance structure, the first resonance frequency can be located to be  $\Omega_0$  rad/sec. The following objective can be defined in terms of  $\omega_0 = \Omega_0 T_s$ , where  $T_s$  is the sampling period in seconds.

$$J = \frac{\int_0^{\omega_0} |G_{\phi,n}(\omega)|^2 d\omega}{\int_0^{\pi} |G_{\phi,n}(\omega)|^2 d\omega} \quad (18)$$

or

$$1 - J = \frac{\int_0^{\pi} |G_{\phi,n}(\omega)|^2 d\omega - \int_0^{\omega_0} |G_{\phi,n}(\omega)|^2 d\omega}{\int_0^{\pi} |G_{\phi,n}(\omega)|^2 d\omega}. \quad (19)$$

The following optimization problem can be used to determine the optimal value of  $n$ .

$$\max_n J \text{ or } \min_n (1 - J) \quad (20)$$

Physically, the objectives imply that the best waveform of  $g_{\phi,n}[k]$  maximizes the proportion of its energy before the first resonance frequency, or minimizes the proportion of its energy after the first resonance frequency, according to an arbitrary move time. For engineering applications, the integral in (20) can be easily approximated by the cumulative summation of the element  $|G_{\phi,n}(\omega)|^2$ . So without any optimization algorithm, the optimal  $n$  can be approximated from the plot of  $J$  or  $(1 - J)$  (20) in terms of  $n$ . The calculation of the optimal scale parameter  $n$  can also be reduced to a scalar bounded nonlinear function minimization problem [13]. So the Matlab routine *fminbnd* in the Optimization Toolbox can be used to find the optimal scale parameter  $n$  very quickly.

Bayo [14], [15] and Singer [16] have studied Gaussian function to generate a continuous-time open-loop driving

function for a flexible manipulator. However, in their studies, the Gaussian function profile or the derivative of the Gaussian function are simply made to start at a small number in the time domain. The tradeoff between the move time and energy concentration of the control profile in the frequency domain is not studied in their work.

#### IV. SIMULATION RESULTS FOR HARD DISK DRIVE SEEK CONTROL

Consider the following flexible system which is embedded in a hard disk assembly, the input is the drive current signal in amp and the output is the position signal in tracks.

$$H(s) = Kc \cdot Kv \cdot Kp \cdot R(s) \frac{1}{s^2}, \quad (21)$$

where  $Kc = 1.3 \frac{\text{tracks/sample}^2}{\text{amp}}$  is a constant gain from current to acceleration,  $Kv = 5 \times 10^4 \frac{\text{samples}}{\text{sec}}$  is the velocity gain,  $Kp = 5 \times 10^4 \frac{\text{samples}}{\text{sec}}$  is the position gain, and  $R(s)$  is a resonance structure. The Bode magnitude plot of a reduced order (28<sup>th</sup>)  $R(s)$  is shown in Fig. 5. This transfer function was derived from the flexible arm of an open disk drive in the Advanced Controls Laboratory at the Oklahoma State University. The resonance modes change drastically due to variation of the mode parameters. On the Bode plot, the peaks of the frequency response may shift in frequency and in amplitude.

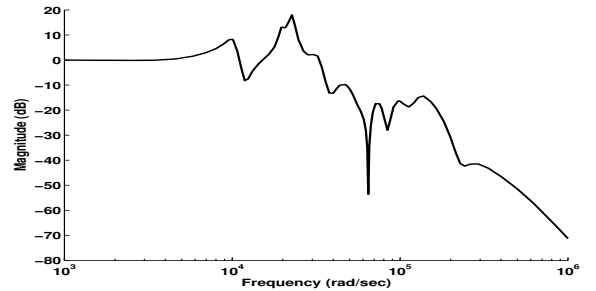


Fig. 5. Bode magnitude of the resonance structure.

Fig. 6 shows the change of the objective  $1 - J$  with  $n$  for  $\Omega_0 = 9.68 \times 10^3$  rad/sec,  $T_s = 2 \times 10^{-5}$  sec and the move time is  $2.5 \times 10^{-3}$  sec. It is clear that the objective is insensitive to the optimal  $n$ . Fig. 7 shows the same information as Fig. 6 with the log scale of  $Y$  axis. In this case,  $n$  is found to be approximately 11.41 and  $1 - J$  is about  $1.0 \times 10^{-5}$ .

With the optimal  $n = 11.41$ , the current signal for a 100 tracks seek can then be calculated. Fig. 8 shows the current signal. Fig. 9 shows the position signal with the full 28<sup>th</sup> resonance model. To see the residual vibration, the position signal near the target track is plotted as shown in Fig. 10.

Fig. 10 shows that the position signal settles within  $\pm 5\%$  track at 2.6 msec which is very close to the move time 2.5 msec. So the input current signal suppresses the residual vibration induced by all the resonance modes.

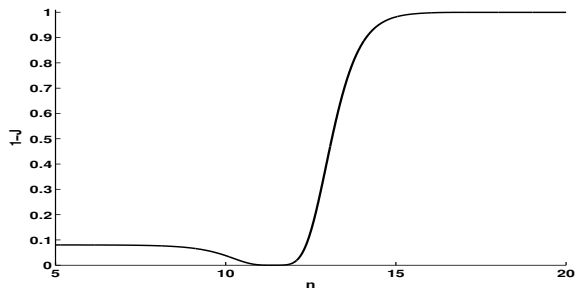


Fig. 6. The change of  $1 - J$  (linear scale) with  $n$ .

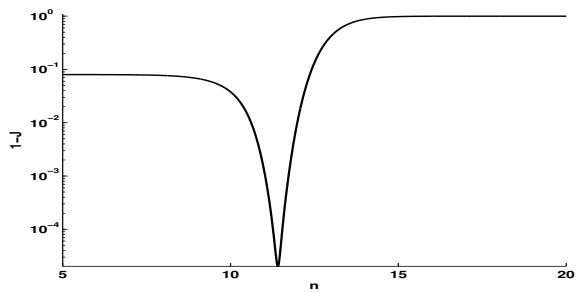


Fig. 7. The change of  $1 - J$  (log scale) with  $n$ .

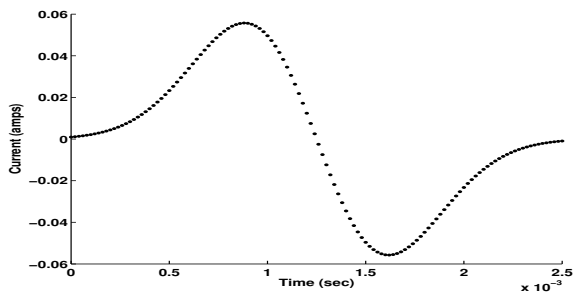


Fig. 8. Current control input signal.

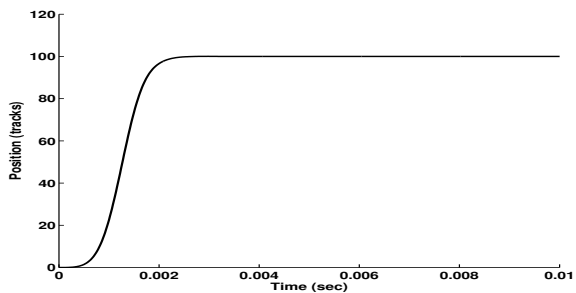


Fig. 9. 100 track seeking position signal.

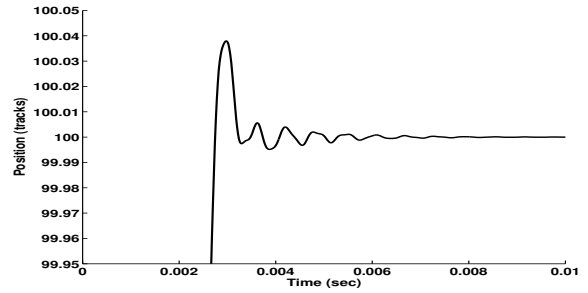


Fig. 10. 100 track seeking position signal near the target.

Next, the current signal will be analyzed from the filter point of view. Fig. 11 shows the reference velocity signal which is the integral of the acceleration signal. This signal is considered as the impulse response of a Finite Response Filter. The magnitude of the frequency response of this Finite Response Filter is shown in Fig. 12. It is clear that this Finite Response Filter has a very good cutoff of high frequency signals.

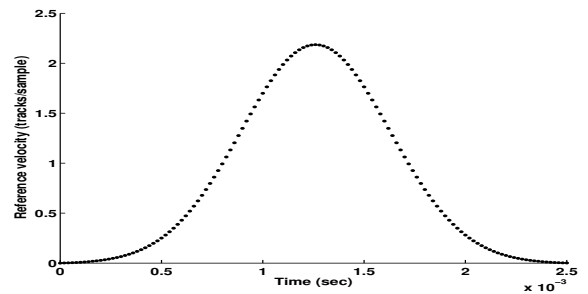


Fig. 11. Reference velocity.

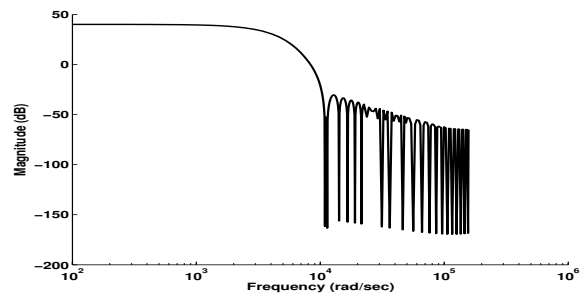


Fig. 12. Frequency response of the Finite Response Filter.

It must be pointed out that the control input move time cannot be arbitrarily reduced if a certain settling time is required. It depends on the resonance characteristics. As shown before, a signal cannot arbitrarily achieve both time and frequency localization. Reducing move time will result a poor frequency concentration. Fig. 13 shows the concentration  $1 - J$  defined in (19) with different move time for the same sampling period and first resonance frequency given before. From Fig. 13, if

the move time of the control input is chosen to be 0.5 msec, the minimal proportion of its energy after the first resonance is about 0.45 which is very poor. There is a tradeoff between the move time of a control input and its concentration in the frequency domain as shown in Fig. 13.

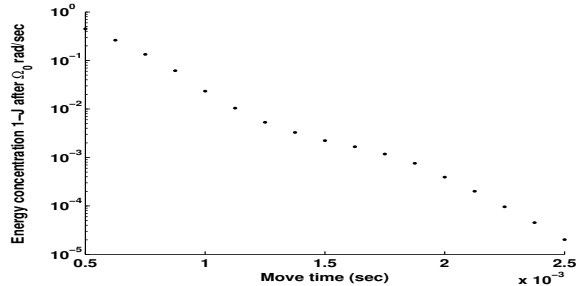


Fig. 13. Concentration  $1 - J$  with different move time.

## V. CONCLUSIONS

In this examination, a robust control profile is generated which suppresses all the resonant dynamics in a flexible dynamic system. This robust control profile is the shifted time-limited version of the functions that optimally achieve the time and frequency localization. The time-limited functions approximate the optimal time-frequency localization property due to the fast decay of functions both in time domain and frequency domain. Given an arbitrary time duration of the control input, the wave form is optimized and analyzed by the filter theory. The simulation results show the effectiveness of this method. The experimental results for closed-loop control using the robust vibration suppression control profile have been studied in [13] and will be reported separately. The methods discussed in this paper are patented (pending) by the Oklahoma State University. Commercial use of these methods requires written permission from the Oklahoma State University.

## VI. ACKNOWLEDGMENTS

This work was supported by the National Science Foundation, grant number 9978748, and Seagate Technology LLC of Oklahoma City, Oklahoma. The authors gratefully acknowledge reviewers' comments.

## VII. REFERENCES

- [1] D. M. Aspinwall, "Acceleration profiles for minimizing residual response," *ASME Journal of Dynamic Systems, Measurement, and Control*, vol. 102, no. 3, pp. 3–6, 1980.
- [2] C. J. Swigert, "Shaped torque techniques," *Journal of Guidance and Control*, vol. 3, no. 5, pp. 460–467, 1980.
- [3] R. C. Thompson, J. L. Junkins, and S. R. Vadali, "Near-minimum time open-loop slewing of flexible vehicles," *Journal of Guidance, Control, and Dynamics*, vol. 12, no. 1, pp. 82–88, 1989.
- [4] S. P. Bhat, "Point-to-point control of linear time invariant dynamical systems: Theory and experiments," Ph.D. dissertation, University of California, Los Angeles, CA, 1990.
- [5] H. Yamamura and K. Ono, "Robust access control for a positioning mechanism with mechanical flexibility," in *Proceedings of the 1st International Conference on Motion and Vibration Control*, Yokohama, Japan, September 1992, pp. 437–442.
- [6] P. H. Meckl and K. Roberto, "Robust motion control of flexible systems using feedforward forcing functions," *IEEE Transactions on Control Systems Technology*, vol. 2, no. 3, pp. 245–253, 1994.
- [7] H. Yamamura and K. Ono, "Vibrationless access control of a positioning mechanism for high-order natural modes of vibration (in Japanese)," *Nippon Kikai Gakkai Ronbunshu, C Hen/Transactions of the Japan Society of Mechanical Engineers, Part C*, vol. 59, no. 559, pp. 727–732, 1993.
- [8] —, "Vibrationless access control of a positioning mechanism for high-order natural modes of vibration (2nd report, vibrationless velocity control) (in Japanese)," *Nippon Kikai Gakkai Ronbunshu, C Hen/Transactions of the Japan Society of Mechanical Engineers, Part C*, vol. 59, no. 568, pp. 3710–3716, 1993.
- [9] —, "Vibrationless access control of a positioning mechanism for high-order natural modes of vibration (3rd report, vibrationless acceleration control) (in Japanese)," *Nippon Kikai Gakkai Ronbunshu, C Hen/Transactions of the Japan Society of Mechanical Engineers, Part C*, vol. 61, no. 585, pp. 1891–1898, 1995.
- [10] Y. Mizoshita, S. Hasegawa, and K. Takaishi, "Vibration minimized access control for disk drives," *IEEE Transactions on Magnetics*, vol. 32, no. 3, pp. 1793–1798, 1996.
- [11] C. K. Chui, *An Introduction to Wavelets*. Academic Press, New York, 1992.
- [12] —, *Wavelets: A Mathematical Tool for Signal Analysis*. SIAM, Philadelphia, 1997.
- [13] L. Zhou, "Robust vibration suppression control profile generation," Ph.D. dissertation, Oklahoma State University, 2004, in preparation.
- [14] E. Bayo and B. Paden, "On trajectory generation for flexible robots," *Journal of Robotic Systems*, vol. 4, no. 2, pp. 229–235, 1987.
- [15] E. Bayo, "Computed torque for the position control of open-chain flexible robots," in *Proceedings of the 1988 IEEE International Conference on Robotics and Automation*, 1988, pp. 316–321.
- [16] N. C. Singer, "Residual vibration reduction in computer controlled machines," Ph.D. dissertation, Massachusetts Institute of Technology, 1988.